Force-feedback micromanipulation with unconditionally stable coupling

Gentiane Venture*, D. Sinan Haliyo†, Stéphane Régnier† and Alain Micaelli*
*Commissariat à l'Energie Atomique,
Laboratoire d'Interface Homme-Machine, BP 6
92265 Fontenay aux Roses, France
E-mail: venture@ieee.org,micaellia@zoe.cea.fr
†Laboratoire de Robotique de Paris,
Univ. Paris 6 - CNRS, BP 61
92265 Fontenay aux Roses, France
E-mail: {haliyo,regnier}@robot.jussieu.fr

***Abstract*— This paper presents a remote handling force feedback coupling for micromanipulation systems. In the litterature, the most generally used coupling mode is 'force-position'. This kind of control scheme is not portable and instability is an often occuring problem. The coupling scheme proposed in this paper is based on the passivity considerations on the teleoperated systems. It is independent of the used haptic interface and the manipulator and unconditionnaly stable regarding scaling ratios. It is experimented using the LRP's (Laboratoire de Robotique de Paris) micromanipulator, which is based on AFM architecture and uses the adhesion forces for pick-up and release tasks. A comparison between the force-position coupling and proposed coupling is presented. Experimental results show the good perfomances in terms of stability.**

***Index Terms*— Micromanipulation, force-feedback teleoperation, passive control.**

I. Introduction

Due to recent development of MEMS and biotechnology, there is a great demand for reliable micromanipulation techniques. Different approaches have been proposed on this purpose [1], but the problem lays on the adhesion phenomena. At this scale, gravitational forces are negligible by comparison to surface forces such as Van der Waals, capillary or electrostatic. Consequently, any microsystem based on the miniaturization of conventional macroscopic gripper encounters a lot of difficulties, for example in releasing an object as it adheres to it. Complex techniques are thus necessary to deal with this phenomenon.

An original approach, that has been developed at LRP, consists in taking advantage of adhesion forces to manipulate objects using a single fingered gripper. This gripper is based on an AFM (Atomic Force Microscopy) probe [2], which allows to combine the sensing and the gripping capabilities. Adhesion based pick-up and release tasks have been validated using a prototype manipulator, called [*mü*]MAD [3]. Recently, vision and force based control schemes have been also implemented [4]. Nevertheless, full autonomous manipulation, except the case of an industrial assembly chain, is very difficult to accomplish and in most cases, user intervention is required.

A state-of-art solution to enhance this user interaction is to use a force-feedback haptic interface. This approach has already been proposed in some works [5], [6]. Its implementation highly depends on the architecture of the manipulator and on its functionalities. Usually, between the haptic interface and the micromanipulator there is only a direct homothetic coupling, where the position of the manipulator is enslaved to the haptic interface's position [7]. In addition, the force coupling is achieved by reflecting the manipulator's force sensor data on the haptic interface with a linear scale ratio. Because of the scale change between micro and macro worlds it is very frequent to need great scaling ratios, generally around 10000 (for micro-to-macro). For different phases of a micromanipulation, it sometimes requires a precise motion (for positioning) or on the contrary, a great travel range (for transportation). If this both tasks are to be controlled through the same haptic interface, it is necessary to adapt the motion scaling, not necessarily on the fly. In these case, instability is an often occurring problem, thus we need a very flexible coupling scheme whose stability would be unaffected by variations on the scaling ratios, guaranteeing the stability robustness. In this aim, a new coupling method is proposed in this paper. This coupling scheme ensures the passivity of the system, and thus its stability. A theoretical and experimental comparison between a direct force-position control and the proposed one is also presented.

II. Experimental set-up

A. Micromanipulator [mü]MAD

The micromanipulation system developed at LRP is built around an active gripper with cartesian architecture. This gripper is an AFM (atomic force microscopy) tipless cantilever beam, mounted on a piezoelectric ceramic which can produce impulses or high frequency sinusoidal waves, generating instantaneous accelerations as high as 10^6 ms^{-2} at the extremity of the AFM cantilever. These dynamical capabilities are used for release and characterization tasks [3]. Due to the AFM sensor, this gripper provides micronewton resolution force measurements. Its vertical displacement is provided by two serial actuators: a nanostage with $12\,\mu m$

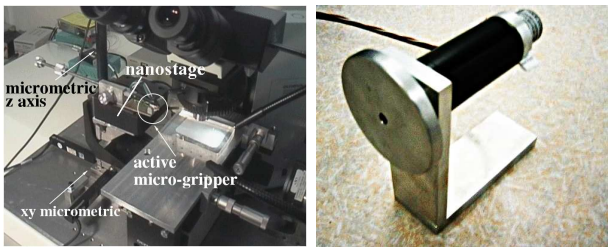

(a) [*mü*]MAD (b) Brigit

Fig. 1. Micromanipulation system (a) and the haptic interface (b)

amplitude and a microstage with sub micrometer resolution and $2.5\,cm$ amplitude. As the only force sensing is on the vertical axis, the force-feedback teleoperation will be implemented on this axis. Hereafter, the micromanipulator will be referred as "slave".

TABLE I

MECHANICAL CHARACTERISTICS OF THE SLAVE

Stiffness of the AFM cantilever	K_{canti}	$21.06\,N/m$
Max. stroke of the microstage	C_{micro}^{max}	$0.002\,m$
Max. stroke of the nanostage	C_{nano}^{max}	$12\,\mu m$

B. Master haptic device: Brigit

Since the teleoperated slave has one DOF on vertical axis, the master device can have either a prismatic or a rotational joint. A prismatic joint appears to be more realistic as it reproduces the kinematics of the slave actuator. Despite this consideration, a rotational joint has some advantages over the prismatic one in this first phase of the project, as it has an unlimited range of movement. Hence, the homothecy between slave and master can be more freely adjusted.

The master device shown in Fig. 1(b) is chosen for this first approach. It is composed by a DC motor equipped with an optical coder and a control wheel. Technical specifications of this device are given in Table II.

Low level control is implemented for rotational velocity (W_M) or current (I_d) control of the master device. The dynamic model of the master is given by:

$$J_M \frac{dW_M}{dt} = R_M F_{op} + K_t I_d - \mu W_M \tag{1}$$

with F_{op} the force applied by the operator on the wheel.

C. Master/slave scaling ratios

As master and slave are to operate in different scales, respectively micro and macro, it is necessary to define the scaling of control parameters between the two devices. The motion of micromanipulator will be controlled by the haptic interface, thus the motion scaling is 'macro to micro'. On the contrary, the force is measured in the microworld and transmitted to the master haptic interface, thus the force scaling is 'micro to macro'.

TABLE II

SPECIFICATION OF THE MASTER DEVICE

Optical Coder	
Resolution	20000 pts/tour
Wheel	
Radius R_M	3.5 cm
DC Motor	
Nominal voltage	42 V
Maximum current I_d^{max}	1.9 A
Torque constant	$52.5\ 10^{-3}$ Nm/A
Maximum torque T_M^{max}	0.1 Nm
Overall	
Friction coefficient μ	$6\ 10^{-6}$
Force/current coef K_t	$5.25\ 10^{-2}$ Nm/A
Total Inertia J_M	$6.523\ 10^{-5}$ kgm^2

The master has been designed for a maximal torque $T_M^{max} = 0.1Nm$. This value ensures a good 'hand held feeling' for the user. The corresponding maximal tangential effort F_M^{max} is given by:

$$F_M^{max} = \frac{T_M^{max}}{R_M} = 2.86N \tag{2}$$

Considering that the maximum flexion of the AFM cantilever would be $12\mu m$, which is the maximum stroke C_{nano}^{max} of the nanostage, maximal measurable force is given by:

$$F_{canti}^{max} = K_{canti} C_{nano}^{max} = 2.52.10^{-4} N \tag{3}$$

Thus, the force scaling ratio is given by:

$$\alpha_f = \frac{F_{canti}^{max}}{F_M^{max}} = 8.8.10^{-5} \tag{4}$$

For the motion scaling, it is necessary to define virtual bounds, as the master's motion is unlimited. These virtual bounds will correspond to $C_{nano}^{max} = 12\mu m$ of the nanostage motion. Choosing $C_M^{max} = 2rad$, approximatively the maximum rotation of a human wrist, ensures that the operator does not need to release it while manipulating.

The motion scaling ratio α_d between the nanostage and the master is thus given by:

$$\alpha_d = \frac{C_M^{max} R_M}{C_{nano}^{max}} = 5800 \tag{5}$$

D. Experimental performances

The haptic interface and the micromanipulator are implemented on separate computers and communicate with a TCP/IP based protocol. This architecture is commonly used in most teleoperation applications and allows ethernet based operation. In this case, the communication goes currently through our laboratory's LAN in order to avoid global

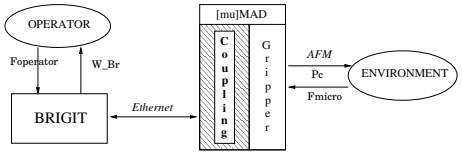

Fig. 2. Structure of the teleoperation system

internet network's imperfections and communication lags. The actual LAN connection enables a sampling period of $T_e = 2ms$ between the two interfaces.

III. Teleoperation of the nanostage

As the control of the nanostage is the most critical part for the manipulation, it is the only actuator considered for the force-feedback coupling in this first phase of our study.

The control scheme proposed here is based on passivity considerations for teleoperated systems and is called position-position bilateral control. It will be hereafter referred as '*PPB*'. It is then compared to a force-position direct haptic control. Table III recapitulates parameters used in the control.

TABLE III
System parameters

P_M,W_M	Measured rotational position/velocity of master
T_M	Torque on master
P_{nano},V_{nano}	Measured position/velocity of nanostage
P_c, V_c	Set-point position/velocity of nanostage
P_{macro}, V_{macro}	position/velocity of nanostage translated in macro world
F_{canti}	AFM measured force

A. PPB control scheme

The architecture of the proposed control has a modular design. Each module is stable when coupled with a passive sub-system, thus the unconditional stability of the overall control scheme can then be guaranteed [8]. The coupling (Fig. 2) is hence composed of three sub-blocks (Fig. 3): the master control block, the homothetic coupling block and the slave control block.

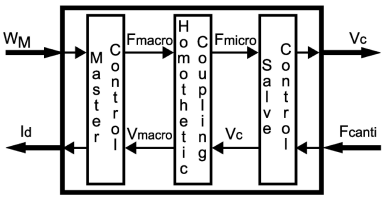

Fig. 3. The *PPB* control scheme decomposition

1) The homothetic coupling block: it is used for macro-to-micro and micro-to-macro conversions, between force F, position P and velocity V data, using force and motion scaling ratios.

$$P_{macro} = \alpha_d P_{nano} \tag{6}$$

$$V_{macro} = \alpha_d V_c \tag{7}$$

$$F_{micro} = \alpha_f F_{macro} \tag{8}$$

2) The master control block: it is a proportional-derivative control of the error on the master position with respect to the slave position converted into macroworld. Inputs are the velocity of the nanostage translated to macroworld V_{macro} and the rotational position and velocity of the master P_M and W_M. Output is the torque on the master T_M, used to calculate the set-point current I_d and also the force on the master F_{macro} which is then sent to slave control through the homothetic coupling block.

$$T_M = K_p \left(P_M - \frac{P_{macro}}{R_M} \right) + K_d \left(W_M - \frac{V_{macro}}{R_M} \right) \tag{9}$$

$$F_{macro} = \frac{T_M}{R_M} \tag{10}$$

$$I_d = \frac{T_M}{K_t} \tag{11}$$

with control parameters K_p and K_d chosen in accordance to the sampling period T_e. Considering the differential equation in P_M obtained with zero as reference position:

$$\frac{J_M}{K_p}\ddot{P}_M + \frac{K_d}{K_p}\dot{P}_M + P_M = 0 \tag{12}$$

The cut-off frequency ω_0 is then given by:

$$\omega_0 = \sqrt{\frac{K_p}{J_M}} \tag{13}$$

With $T_e = 2ms$, the sampling frequency is $f_e = 500Hz$. The bandwidth ω_{BP} is given by:

$$\omega_{BP} = \frac{2\pi f_e}{10} = 314 rad.s^{-1} \tag{14}$$

Necessarily, $\omega_0 < \omega_{BP}$. We have thus chosen $\omega_0 = 100\, rad.s^{-1}$. Accordingly, K_p is computed as follow:

$$K_p = J_M \omega_0^2 = 0.652 \tag{15}$$

Choosing the damping ratio $\zeta = 1$ in order to limit the over-shooting, K_d is then given by:

$$\frac{2\zeta}{\omega_0} = \frac{K_d}{K_p} \Longrightarrow K_d = \frac{2\zeta K_p}{\omega_0} = 0.013 \tag{16}$$

3) The slave control block: it is based on the comparison of the master force translated in the micro world F_{micro}, and the cantilever contact force F_{canti} (17) in a control force loop. Output is the set-point velocity V_c of the nanostage. This parameter is sent back through the homothetic coupling block. As the nanostage is controlled on position, P_c is computed by integrating V_c with saturation levels at 0 and $12.10^{-6}m$, travel limits of the nanostage (Table I).

$$V_c = K(F_{micro} + F_{canti}) \tag{17}$$

where K is the enslaving gain. Simulations shows that good performances are achieved with $K = 3$

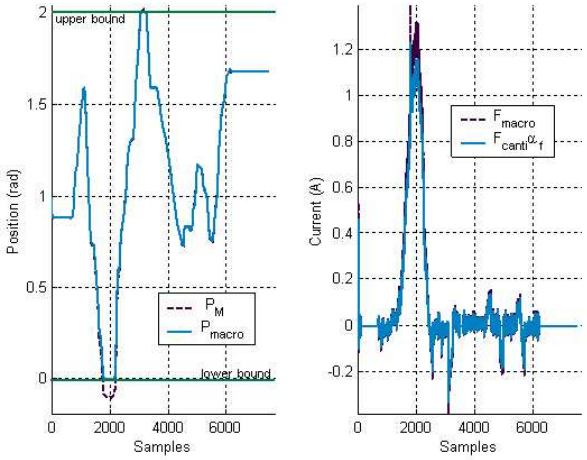

Fig. 4. Results for the passive control *Sampling period = 2ms*

4) Algebraic loop: As stated above, V_c is used both for position control of the nanostage in slave control and for position control of Brigit in master control. This approach causes an algebraic loop to appear in the expression of V_c. This loop is unstable when working with real time sampling.

$$V_{c_{k+1}} = AV_{c_k} + BW_{M_k} + CInt_k - KF_{canti_k} \tag{18}$$

Where:

- $Int_k = P_{M_k} - \dfrac{P_{macro_k}}{R_M}$
- $|A| = \dfrac{KK_d\alpha_f\alpha_d}{R_M^2} = 16.39 > 1 \Longrightarrow$ instability
- $B = \dfrac{KK_d\alpha_f}{R_M}, \quad C = \dfrac{KK_p\alpha_f}{R_M}$

For its implementation, we propose to solve this algebraic loop by considering that $V_{c_{k+1}} = V_{c_k}$ in (18). We then obtain:

$$V_{c_{k+1}} = AV_{c_{k+1}} + BW_{M_k} + C.Int_k - K.F_{canti_k} \tag{19}$$

$$V_{c_{k+1}} = \frac{R_M KK_d\alpha_f}{R_M^2+KK_d\alpha_f\alpha_d}W_{M_k} + \frac{R_M KK_p\alpha_f}{R_M^2+KK_d\alpha_f\alpha_d}Int_k - \frac{KR_M^2}{R_M^2+KK_d\alpha_f\alpha_d}F_{canti_k} \tag{20}$$

B. Experimental results

This control algorithm has been tested both in simulation and experimentally. The simulator has been obtained by identification of the dynamic properties of each component of the system, through their transfer functions and dynamic models. As they are in very good agreement, only the experimental results are presented (Fig.4). Master and slave interfaces motions fit very closely, as well as the measured micro-forces and the force-feedback. Note that when the slave reaches one of its boundaries, it is also reflected through the haptic interface.

C. Comparison with force-position control

1) Force-position control: Force-position direct haptic control is adopted in most tele-micromanipulation works [9]. We have implemented such a control on our system in order to compare its performances with the proposed *PPB* control. This direct coupling is established such as the position of the nanostage P_c is proportional to the master position while the force applied on the master though the current I_d is proportional to the AFM measured contact force.

$$P_c = \frac{P_M R_M}{\alpha_d} \tag{21}$$

$$I_d = \frac{F_{canti}R_M}{K_t\alpha_f} \tag{22}$$

2) Comparisons: we first quantitatively compare the two controls for the teleoperation. The unconditional stability of each master-slave coupling is compared using the Llewelyn criteria [10], applied to a two port system as shown in Fig. 5, using (23), (24), (25), (26), as used in [11] and [12].

$$\begin{bmatrix} V_i \\ V_o \end{bmatrix} = \begin{bmatrix} Z_{Q11} & Z_{Q12} \\ Z_{Q21} & Z_{Q22} \end{bmatrix} \begin{bmatrix} F_i \\ F_o \end{bmatrix} \tag{23}$$

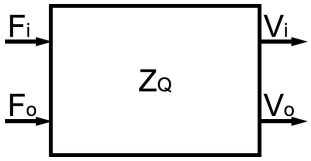

Fig. 5. Two-port impedance model

The two-port impedance system is passive and unconditional stability is ensured if the following Llewelyn criteria are all true:

$$Re(Z_{Q11} \geq 0) \tag{24}$$

$$Re(Z_{Q22} \geq 0) \tag{25}$$

$$2Re(Z_{Q11})Re(Z_{Q22}) \geq |Z_{Q12}Z_{Q12}| + Re(Z_{Q12}Z_{Q12}) \tag{26}$$

We compute the Llewelyn criteria for both systems; where in (23):

$$F_i = F_{op},\ F_o = F_{canti},\ V_i = W_M \text{ and } V_o = V_{canti}.$$

The chosen frequency range is $[0\ 50]Hz$ ($[0\ 300]rad.s^{-1}$), according to the bandwidth ω_{BP} given in (14). Each criterion is plotted in Fig. 6 and Fig. 7, with first row: $Re(Z_{Q11})$, second row: $Re(Z_{Q22})$ and third row: $2Re(Z_{Q11})Re(Z_{Q22}) - |Z_{Q12}Z_{Q21}| - Re(Z_{Q12}Z_{Q21})$.

Fig. 6 shows that the force-position direct homothetic coupling does not implies unconditional stability and passivity, as all three conditions are not always satisfied and criterion have negative values. On the contrary, Fig. 7 shows that the coupling with the proposed *PPB* control is unconditionally

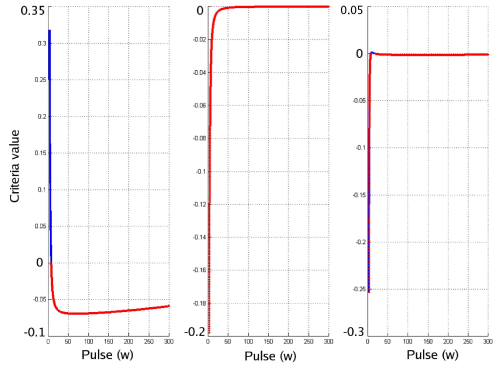

Fig. 6. Llewelyn criteria for the force-position control

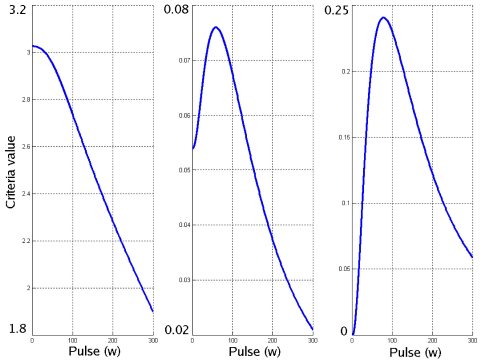

Fig. 7. Llewelyn criteria for the *PPB* control

stable: the three criteria are always positive and satisfied. This implies that the stability would not be affected even if scaling ratios α_f and α_d are changed. The system consequently has a robust stability.

Using [*mü*]MAD, we experimentally compare the behavior and performances of both controls first with the above chosen force scaling ratio then with a the force scaling ratio divided by 10: $\alpha'_f = 8.8.10^{-6}$. Thus the contact force feeling is amplified on the master (9) so is the pull-off force. In the first case, both controls have a stable behavior and results are nearly identical. However, the force feeling on the master is weak and for example the pull-off phenomena is nearly unnoticed. The results for the α'_f are shown on Fig. 8 for *PPB* control and Fig. 9 for force-position coupling. For the *PPB* control, the force feeling is firmer and well transmitted. The weak pull-off force is felt by the user, as it can clearly be seen in motion plots and the system is still perfectly stable. On the contrary, Fig. 9 shows that for the force-position control, instability occurs as soon as the measured forces in non-zero. The dependency of this kind of coupling to the scaling ratios has also been shown in [7].

From the point of view of a user, two important behaviors can be examined between the coupling schemes: the damping behavior and the bounds management, as the nanostage has $12\mu m$ travel range and the master has an unlimited one.

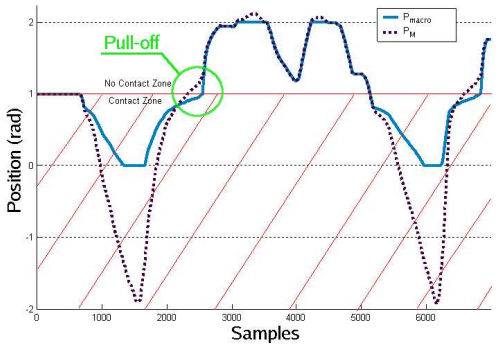

Fig. 8. Influence of the force scaling ratio α_f on the *PPB* control *Sampling period* = $2ms$

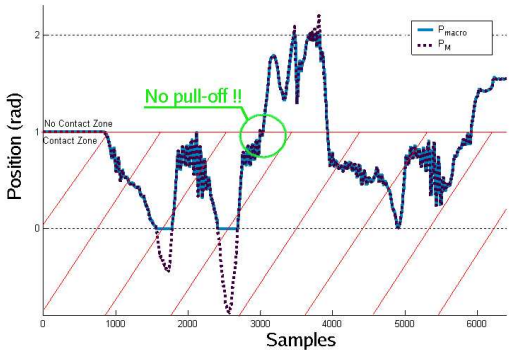

Fig. 9. Influence of the force scaling ratio α_f on the force-position control *Sampling period* = $2ms$

For the bounds management, it is intrinscally impossible in the case of the force-position control, as the measured force is null so no information is reflected through the force-feedback. In case of the *PPB* control, as the vleocity V_c is controlled fed back through the haptic coupling (Fig. 10).

To study the damping behavior of the system the AFM tip is brought into contact and pushed into the substrate. The master is released by the user ($F_{op} = 0$). Both positions of the master and the nanostage are studied. In case of the *PPB* control (Fig. 11) the system has a strong damping coefficient: the master and the slave stop before reaching the upper bound of the nanostage, as soon as the AFM is no longer in contact. In the case of the force-position control, the gripper shots up as soon as the master is released, reaches the upper bound then bounce down again. This behavior is due to the fact that the only damping is the real friction μ of the master device.

IV. Conclusion

We have presented an efficient control designed for a teleoperated micromanipulator. It is based on passivity considerations on the frequencies range. This control provides more robustness than common force-position control, as it is unconditionally stable. It also allows increasing the perfor-

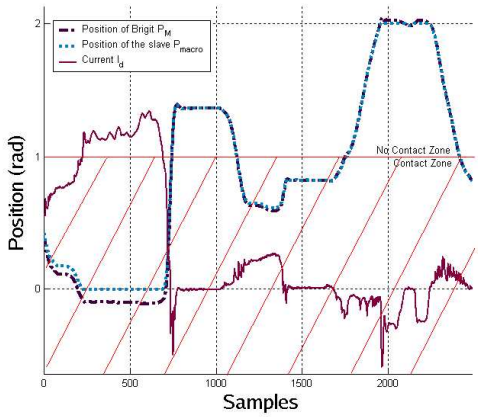

Fig. 10. Bounds of the slave on the master, *PPB control Sampling period = 2ms*

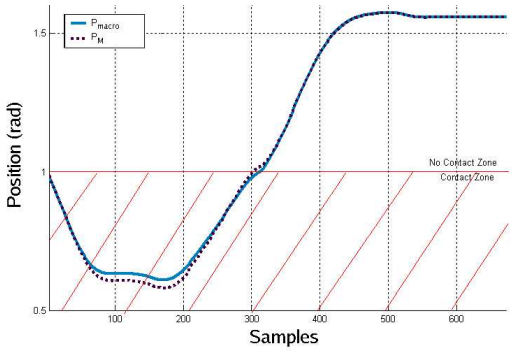

Fig. 11. Damping behavior of the system with the *PPB control Sampling period = 2ms*

mances such as the feeling of the bounds and the damping coefficient between the master and the slave. Moreover, it is also possible, if using an energetic filter, to change the scaling ratios on the fly without losing the stability properties as proposed in [13] and [14].

These results have been obtained on our experimental system with a one degree of freedom haptic device for master. Pick-up, rolling and release operations of ragweed pollens (diameter=$20\mu m$) are experimented (Fig. 12). During this experiments, users is perfectly able, through the force-feedback, to feel the stiffness of pollens when compressed and rolled, as well as the pull-off and adhesion forces during release.

The proposed coupling can be very easily applied to any micromanipulator and haptic interface. Further works will then concern the coupling of the other actuators of the micromanipulator on a single three degrees of freedom haptic device.This kinematic redundancy would combine the very precise motion (nanostage) with great travel range (microstages) in 3D workspace. Teleoperation of the horizontal

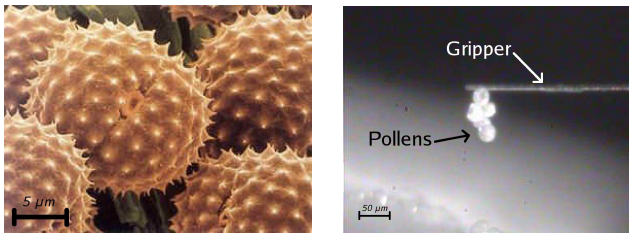

Fig. 12. Manipulation of ragweed pollens

motion would be interesting for user guidance for example in case of path planning [15].

REFERENCES

[1] J.A. Thompson and R.S. Fearing, "Automating microassembly with ortho-tweezers and force sensing," in *Proc. of IROS: IEEE/RSJ International Conference on Intelligent Robots and Systems*, 2001.

[2] D.S. Haliyo and S. Régnier, "Manipulation of micro-objects using adhesion forces and dynamical effects," in *Proceedings of ICRA/IEEE International Conference on Robotics and Automation*, May 2002.

[3] D.S. Haliyo, S. Régnier, and J-C. Guinot, "[m]mad, the adhesion based dynamic micro-manipulator," *European Journal of Mechanics A/Solids*, vol. 22 (6), pp. 903–916, 2003.

[4] F. Dionnet, D.S. Haliyo, and S. Rgnier, "Autonomous micromanipulation using a new strategy of accurate release by rolling," in *Proceedings of ICRA/IEEE International Conference on Robotics and Automation*, 2004.

[5] N. Ando, P. Korondi, and H. Hashimoto, "Development of micro-manipumator and haptic interface for networked micromanipulation," *IEEE/ASME Trans. on Mechatronics*, vol. 6, no. 4, pp. 417–427, 2001.

[6] S. Guo, K. Sugimoto, and S. Hata, "Complex control for a human scale tele-operating system for micro-operation, vancouver, canada," in *Proc. of IEEE International Symposium of Intelligent Control*, 2002, pp. 25–30.

[7] L.F. Peñín, M. Ferre, J. Fernandez-Pello, R. Aracil, and A. Barrientos, "Design fundamentals of master-slave systems with force-position bilateral control scheme," in *Proc. of the Fifth IFAC Symposium of Robot Control*, September 1997, pp. 631–638.

[8] R.J Anderson and M.W. Spong, "Bilateral control of teleoperators with time delay," *IEEE Trans. on Automatic Control*, vol. 34, no. 5, pp. 494–501, 1989.

[9] S. Grange, F. Conti, P. Helmer, P. Rouiller, and C. Bauer, "The delta haptic device as a nanomanipulator," in *SPIE Microrobotics and Microassembly III, Boston MA, USA*, November 2002, pp. 164–166.

[10] F.B. Llewellyn, "Some fundamental properties of transmission systems," in *Proc.of IRE*, 1952, vol. 40, pp. 271–283.

[11] R. Adams and B. Hannaford, "A two-port framework for the design of unconditionally stable haptic interfaces," in *Proceedings of IROS*, 1998, pp. 1254–1259.

[12] K. Hashtrudi-Zaad and S.E. Salcudean, "Analysis of control architectures for teleoperation systems with impedance/admittance master and slave manipulators," *Int. Jour. Robotic Reseach*, vol. 6, no. 20, pp. 419–445, 2001.

[13] G. Hannaford, B.and Hirzinger, C. Preusch, and J.H. Ryu, "Time domain passivity control with reference energy behavior," in *IEEE/RSJ International Conference on Intelligent Robots and Systems*, 2003.

[14] G. Niemeyer, *Using Wave Variables in Time Delayed Force Reflection Teleoperation,*, Ph.D. thesis, Massachusetts Institute of Technology, September 1996.

[15] A. Ferreira, C. Cassier, and S. Hirai, "Automated microassembly system assisted by vision servoing and virtual reality," *IEEE/ASME Transactions on Mechatronics*, vol. 9, no. 2, 2004.